ELSEVIER

Contents lists available at ScienceDirect

Biosensors and Bioelectronics

journal homepage: www.elsevier.com/locate/bios





Simultaneous colorimetric and electrochemical detection of trace mercury (Hg^{2+}) using a portable and miniaturized aptasensor

Ana M. Ulloa-Gomez^a, Alec Lucas^a, Abbey Koneru^a, Amit Barui^a, Lia Stanciu^{a,b,*}

ARTICLE INFO

Keywords: Dual-modality Multiplexing Electrochemical Colorimetric On-site

ABSTRACT

We report a novel aptasensor for the simultaneous colorimetric and electrochemical detection of mercury (Hg²⁺). This device consists of a paper-based microfluidic component (µ-PAD) incorporated into a miniaturized threeelectrode system fabricated through printed circuit board (PCB) technology. This biosensor is portable, rapid, versatile, and can detect Hg²⁺ down to 0.01 ppm based on 3 σ of the blank/slope criteria. Moreover, it is highly selective against As²⁺, Cu²⁺, Zn²⁺, Pb²⁺, Cd²⁺, Mg²⁺, and Fe²⁺, reaching up to 13 times more of the input signal than the other heavy metals. The colorimetric detection mechanism uses aptamer functionalized polystyrene (PS)-AgNPs and Ps-AuNPs microparticles' specific aggregation. The Ps-AuNPs-based system allows qualitative detection (LOD 5 ppm) and stability over seven days (up to 97.59% signal retention). For the Ps-AgNPs-based system, the detection limit is 0.5 ppm with a linear range from 0.5 to 20 ppm (adjusted $R^2 = 0.986$) and stability over 30 days (up to 94.95% signal retention). The electrochemical component measures changes in charge transfer resistance upon target-aptamer hybridization using a [Ru (NH₃)₆]³⁺Cl₃] redox probe. The latest component presents a linear range from 0.01 to 1 ppm (adjusted R²= 0.935) with a LOD of 0.01 ppm and performance stability over seven days (up to 102.52 ± 11.7 signal retention). This device offers a universal dual detection platform with multiplexing, multi-replication, quantitative color analysis, and minimization of false results. Furthermore, detection results in river samples showed recoveries up to 91.12% (RSD 0.85) and 105.61% (RSD 1.62) for the electrochemical and colorimetric components, respectively. The proposed system is highly selective with no false-positive or false-negative results in an overall wide linear range and can safeguard the accuracy of detection results in aptasensing platforms in general.

1. Introduction

Heavy metals are significant environmental pollutants naturally found in the earth's crust. Cobalt (Co), copper (Cu), chromium (Cr), iron (Fe), magnesium (Mg), and zinc (Zn) are essential nutrients that are required for biochemical processes (Arif et al., 2016). However, mercury (Hg), arsenic (As), cadmium (Cd), chromium (Cr), and lead (Pb) are highly carcinogenic toxins that have caused significant health concerns due to their abundance in the environment. Mercury is a neuro and nephron-toxin, and according to the World Health Organization, elemental mercury vaporizes readily, and it can stay for up to a year in the atmosphere, where it ultimately settles in the sediment of water bodies. Other significant sources include anthropogenic activities such as agriculture, mining, incineration, and industrial wastewater discharges (Jaishankar et al., 2014). Therefore, continuous mercury

monitoring has gained attention in the past decades.

Analytical methods such as cold vapor atomic absorption spectrometry, cold vapor atomic fluorescence spectroscopy, inductively coupled plasma mass spectroscopy, and x-ray and visible spectrophotometry are commonly used to detect mercury (Chwastowska et al., 2005; Wen et al., 2002) Despite their remarkable sensitivity and selectivity, these are still complex lab-based methods, require extensive sample preparation, trained personnel, and are unsuitable for on-site detection. To overcome these problems, colorimetric and electrochemical biosensors have been developed to allow user-friendly and portable testing (Yan et al., 2021). Nevertheless, nearly all the reported approaches are carried out in solution or present a short linear working range, limiting their on-site use and increasing overall costs. Furthermore, some platforms suffer from interferences from other metal ions leading to false detection results (Lee et al., 2007; T. Li et al., 2009; Tao

a Department of Materials Engineering, Purdue University, West Lafayette, IN, 47907, United States

^b Birck Nanotechnology Center, Purdue University, West Lafayette, IN, 47907, United States

^{*} Corresponding author. Department of Materials Engineering, Purdue University, West Lafayette, IN, 47907, United States. E-mail address: lstanciu@purdue.edu (L. Stanciu).

Li et al., 2009; Xuejia Xue et al., 2008). For instance, the EPA-USA annual waste testing reported mercury in soil with a false positive rate of 6% (Bruce and Richards,). Furthermore, the USA-Ecology department found many false positives when using X-ray fluorescence to analyze metal analytes such as antimony, As, Cd, Co, Pb, Hg, and molybdenum (Office of water regulations and standards Washington, 1988). Hence, developing a new highly selective platform for Hg²⁺ detection that minimizes false positive and negative results and provides wide linear range is of significant interest to the field.

Recently, microfluidic paper-based analytical devices (μ-PADs) have been widely used to develop colorimetric platforms. These platforms bring many advantages, including cost-effectiveness, disposability, simple fabrication, low sample volume required, and ease of storage (Abdollahi-Aghdam et al., 2018). A variety of metallic-based nanoparticles have been used for this purpose, but especially those modified with aptamers have gained more attention due to their high selectivity and sensitivity. Aptamers are short single-stranded DNA or RNA oligonucleotides obtained through a randomized selection process called systematic evolution of ligands by exponential enrichment (SELEX) and have been selected due to their high affinity towards specific analytes. Furthermore, compared to other biomolecules, such as antibodies, aptamers exhibit outstanding characteristics such as the ability to recognize small molecules and higher stability over a wider range of ionic conditions, temperature, and pH(Friedman et al., n.d.; Kulabhusan et al., 2020). In the case of the DNA aptamers used for mercury detection, the target can bind specifically to the N₃ domain and bridge the two thymidine residues to form stable metal-mediated DNA duplexes N₃-T-Hg-T-N₃ (Cao et al., 2009a; Chen et al., 2014a; Han et al., 2009; Lee et al., 2007; Song et al., 2017). Another advantage of these biomolecules is that they can be easily modified with alkanethiol linkers and used in the covalent immobilization on gold surfaces, forming a stable monolayer. The monolayer formation allows their use on different electrochemical techniques such as impedance spectroscopy, cyclic and square wave voltammetry, and chronoamperometry (Han et al., 2009; Oberhaus et al., n.d.). Nevertheless, most of these electrochemical platforms have been developed in standard three-electrodes systems, which represents a drawback for on-site detection, and limits their commercialization as they are not easy to manufacture on a large scale (Cao et al.,

Among metallic-based nanomaterials, gold (AuNPs) and silver nanoparticles (AgNPs) have been widely used because of their exceptional optoelectrical and chemical properties (Chansuvarn et al., 2015). Indeed, several functionalized gold and silver nanoparticles applications for mercury detection has been the focus of research in the last decades (Chansuvarn et al., 2015; Chen et al., 2014a; Miyake et al., 2006; Song et al., 2017; Tanvir et al., 2019a, 2019b; Zarlaida and Adlim, 1967). For both nanoparticles systems, when the surface charge of dispersed AuNPs and AgNPs approaches neutralization or a specific target-aptamer binding event takes place, the distance between nanoparticles (NPs) is reduced, and surface plasmon coupling occurs. This phenomenon results in a redshift in the absorbance wavelength of colloidal NPs and a color change. The degree to which this color change is a quantitative indicator of mercury concentration. However, the colorimetric sensing mechanism based on silver nanoparticles (AgNPs) is not only aggregation based; the oxidation of Ag° to Ag⁺ is promoted by the Hg²⁺, which changes the size of the nanoparticles, shortening the wavelength and causing a yellow to white color transition (Firdaus et al., 2017; Tanvir et al., 2019a; Zarlaida and Adlim, 1967).

While electrochemical and colorimetric units including into one single system, with various heavy metals as targets were previously reported (Chaiyo et al., 2016; Ejeta and Imae, 2021), the targets were either different from mercury (e.g. cadmium, copper, or chromium), or used the electrochemical and colorimetric units to detect a different target individually. Moreover, none of these reports uses aptamer-based recognition. Thus, to the best of our knowledge, herein we report for the first time on the dual electrochemical and colorimetric (µ-PAD)

aptamer-based detection of mercury within one biosensing device. This work highlights novel bio-functional materials via aptamer functionalization, and their integration in a dual detection aptasensor that contains both a smartphone-based paper test that detects mercury in a wide linear range and accurately uses an imaging application and accurate color analysis to register color change, and an electrochemical sensor that measures changes in the resistance of a gold miniaturized electrode. Moreover, we put forward two colorimetric detection mechanisms: one is based on the surface plasmon resonance-induced color change of gold nanoparticles AuNPs (Chen et al., 2014b), while the other uses silver nanoparticles (AgNPs). The strength of these simultaneous detection modalities results in a rapid mercury screening test that and can be used for on-site detection without the need for complicated equipment and trained technicians. Finally, by checking for mercury presence in river water with this dual detection aptasensing device, we reduce the likelihood of false positive or false negative results, which is a known challenge for such rapid tests.

2. Methodology

2.1. Materials

Phosphate buffer solution 0.01 M (pH 7.4 at 25 °C), tris(2-carboxyethyl) phosphine hydrochloride, 6-mercaptohexanol (MCH), hexaammineruthenium (III) chloride, glycerin, polystyrene latex beads (0.46 μm average diameter), gold (III) chloride trihydrate (99.9%), trisodium citrate dihydrate, sodium borohydride, silver nitrate, bovine serum albumin (BSA) and standards solutions of 1000 mg/L mercury, lead, cadmium, arsenic, zinc, iron, magnesium, and copper were procured from Sigma Aldrich. Black Xerox $^{\rm TM}$ ColorQube 8570/8580 series wax ink was purchased in Xerox. Tris-EDTA buffer pH 7.5 was purchased in Integrated DNA Technology (IDT). Acetone and ethanol were purchased in Fischer Scientific. The pH was adjusted with 1 M NaOH and 1 M HCl for all the solutions. All the glassware used was cleaned in Aqua regia solution (3:1 of hydrochloric acid: nitric acid), rinsed with DI water, and dry with N_2 before use.

Single-stranded DNA (ssDNA) oligos normalized to 100 μ M in IDTE buffer pH 8.0 were purchased in Integrated DNA Technology (IDT). The two aptamer sequences used were as follows (L. Li et al., 2009):

- ssDNA: 5'-TTT-TTT-TT-T-3' for Ps-AuNPs and Ps-AgNPs microparticles immobilization
- Thiolated-ssDNA:/5ThioMC6-D/TTT-TTT-TTT-T-3' for immobilization on the gold working electrode

Thymine-rich ssDNA was used as the aptamer of Hg²⁺, as it can strongly bind to thymine and form T-Hg-T complexes. Furthermore, ssDNA can uncoil sufficiently to expose their bases in comparison to dsDNA, which only exposes the negatively charged phosphate-backbone. This favors the electrostatic interaction of ssDNA with citrate-capped silver and gold nanoparticles, which ultimately leads to a strong absorption on the unmodified nanoparticles (L. Li et al., 2009).

2.2. Synthesis of Ps-AuNPs decorated with ssDNA

To prepare gold-based microparticles, 100 μ l of polystyrene beads (Ps) (\sim 0.46 μ m average diameter) from the original stock solution were mixed with 4 ml DI water and sonicated for 15 min. Then, 8 ml of DI water and 63.4 μ l of 254 mM gold (III) chloride trihydrate in DI water solution were added to the Ps solution and stirred for 5 min at 300 rpm at room temperature (RT). Next, 20 ml of DI water and 82.86 mg of trisodium citrate dihydrate were added to the solution. Finally, 13.84 ml of DI water were added to obtain a final concentration of 0.35 mM for gold (III) chloride trihydrate and 6.125 mM for trisodium citrate dihydrate. The solution was stirred at 750 rpm for 30 min at RT followed by heat treatment in a glycerol bath at 95 °C for 20 min without stirring. Then,

the Ps-AuNPs microparticles were washed by separating the solution in 1.2 ml per 1.5 ml centrifuge tubes and placing the tubes in an Eppendorf centrifuge 5810 R (15-amp version) at 7000 rpm for 1 h at 20 $^{\circ}\text{C}$. After centrifugation, the supernatant was removed, and the particles were resuspended in DI water and stored at 4 $^{\circ}\text{C}$.

To immobilize ssDNA, Ps-AuNPs solution with an optical density (OD) of 0.25 was centrifuged and resuspended in TE buffer (pH 5.5). ssDNA aliquots were taken out from $-20\,^{\circ}\text{C}$ and left in an ice bucket to slowly thaw. Then, the aliquots were placed in a heat block at 95 $^{\circ}\text{C}$ for 3 min and quenched. Finally, 133 μl of 100 μM ssDNA was added per 2 ml Ps-AuNPs of an OD of 0.25 at 530 nm wavelength and left stirring for 24 h at 4 $^{\circ}\text{C}$. To block the microparticles' surface and prevent unspecific target-binding, 6.2 μl of 0.35 wt % BSA in PBS was added per 2.133 ml Ps-AuNPs-ssDNA solution and stirred for 30 min at 4 $^{\circ}\text{C}$. After blocking the Ps-AuNPs-ssDNA microparticles with BSA, a final washing step took place. The supernatant was removed, and the blocked particles were resuspended in TE buffer pH 7.5 and stored at 4 $^{\circ}\text{C}$.

2.3. Synthesis of Ps-AgNPs decorated with ssDNA aptamers

To prepare silver-based microparticles, 100 μ l of polystyrene beads (~0.46 μ m average diameter) from the original stock solution were mixed with 4 ml DI water and sonicated for 15 min. Then, 10 ml of DI water, 27.4 μ l of 588.68 mM silver nitrate (AgNO₃) in DI water solution, and 1.407 ml of 200 mM sodium borohydride in DI water were added to the Ps solution and stirred for 5 min at RT. Then, 20 ml of DI water and 1.41 ml of 200 mM trisodium citrate dihydrate. Finally, 9.06 ml of DI water were added to obtain a final concentration of 0.35 mM and 6.125 mM for AgNO₃ and trisodium citrate dihydrate, respectively. The solution was stirred at 700 rpm for 1 h at RT. Then, microparticles were washed by separating the solution in 1.2 ml per 1.5 ml centrifuge tubes and centrifuging at 7000 rpm for 1 h at 20 °C. After centrifugation, the supernatant was removed, and the particles were resuspended in DI water. To immobilize ssDNA, Ps-AgNPs solution with an OD of 0.39 was

centrifuged and resuspended in TE buffer pH 5.5. ssDNA aliquots were taken out from $-20\,^{\circ}\text{C}$ and left in an ice bucket to thaw slowly. Then, the aliquots were placed in a heat block at 95 $^{\circ}\text{C}$ for 3 min and quenched. Finally, 133 μ l of 100 μ M ssDNA were added per 2 ml Ps-AgNPs of an OD of 0.39 at 390 nm wavelength and left stirring for 24 h at 4 $^{\circ}\text{C}$. To block the microparticles' surface and prevent unspecific target-binding, 6.2 μ l of 0.35 wt % BSA in PBS was added per 2.133 ml Ps-AgNPs-ssDNA solution and stirred for 30 min at 4 $^{\circ}\text{C}$. After blocking the Ps-AgNPs-ssDNA microparticles with BSA, a final washing took place at 4 $^{\circ}\text{C}$. The supernatant was removed, and the blocked particles were resuspended in TE buffer pH 7.5 and stored at 4 $^{\circ}\text{C}$.

2.4. Design and fabrication of the $\mu\text{-PAD}$ device and three-electrode system

The developed hybrid sensor is composed of 2 major sections viz. (a) a μ -Pad paper device and (b) an electrochemical sensor system (Figure S. 1). The microfluid wax-printed device was designed in Adobe Illustrator (Adobe Systems, INC.). The wax pattern was printed on Whatman 1 grade filter paper using a XeroxTM-Color solid wax printer (ColorQube 8570). The μ -PAD device was then heat-treated at 90 °C for 1–3 min using a Thermo Scientific (HERAtherm ref. 51028118) oven. As Shown in Figure S1a, the pattern consisted of four circles, in which two were assigned as testing areas (~2.5 mm diameter) and two as reference/control areas (diameter). The two testing areas are connected through a ~0.5 mm width channel leading to the three-electrode system's working electrode. Finally, double-sided tape was used to incorporate the μ -PAD device into the electrochemical circuit.

The electrochemical miniaturized three-electrode system was designed in KiCAD/PCBnew app and ordered in PCBway. The detailed design of the developed sensor is depicted in Figure S. 1b. The electrochemical sensor is composed of a working (WE), a counter (CE), and a reference (RE) electrode. The electrodes use 150 μ m Polyimide Flex material as the substrate and are composed of 70 μ m thick copper as the

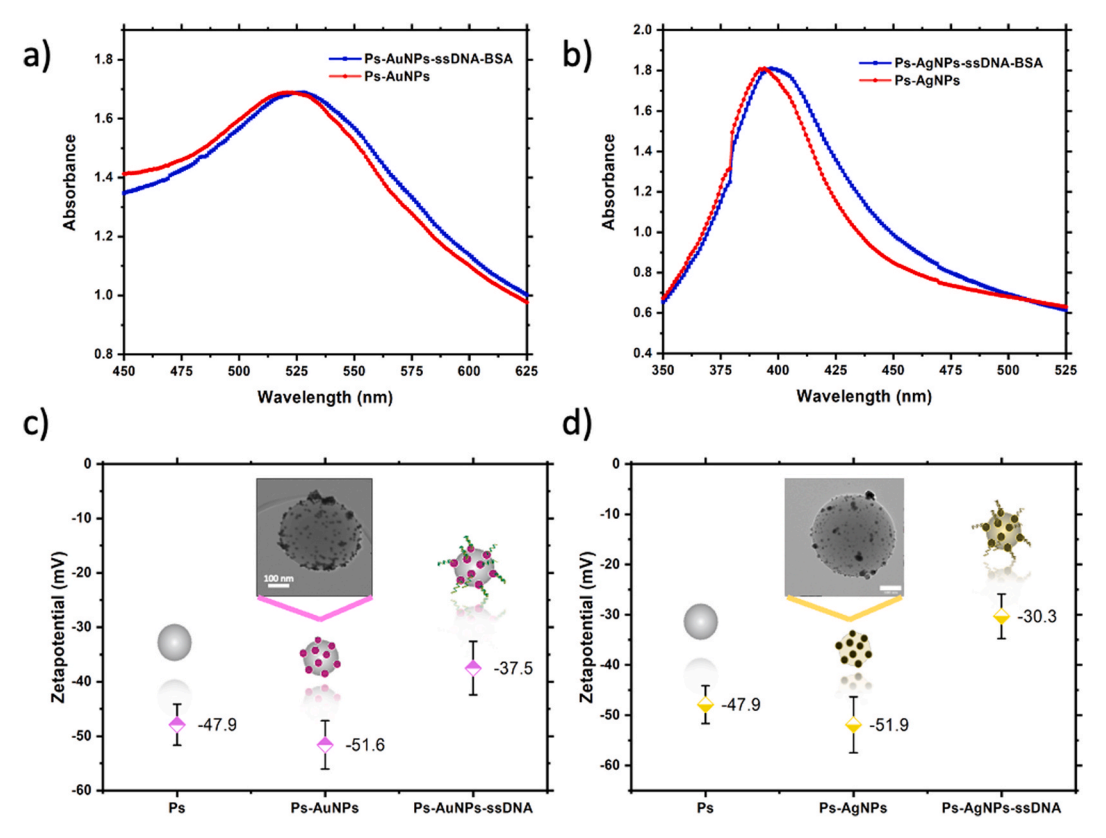


Fig. 1. UV-vis spectra and zeta-potential values of Ps-AuNPs (a and c) and Ps-AgNPs (b and d) modified microparticles with and without DNA.

base material with 77 nm and 109 nm coating of immersion gold and silver, respectively. Prior to any surface modification, printed circuit board (PCB) devices were sonicated for 15 min in acetone, 15 min in ethanol, and 10 min in DI water to clean the surface. Finally, N₂ was used to dry the surface, and the sensors were stored in a nitrogen chamber at RT until use. To obtain a pseudo-reference electrode that could be incorporated into the hybrid system, silver PCB electrodes were cleaned and immersed in 7.5% sodium hypochlorite for 10 min at RT as previously reported (Moschou et al., 2015). A color change was observed after this stage from silver to dark brown/gray (Figure S. 6 b inlet real picture), visually indicating that a surface chlorination (AgCl) layer is formed on top of the Ag plating (Moschou et al., 2015; Papamatthaiou et al., 123AD). Then, the electrodes were rinsed with DI water, dried with N₂, and left in 10 mM PBS solution at RT until use.

To modify the gold WE, 100 μM thiolated ssDNA stock solution was thawed, heated at 95 °C for 3 min, and quenched in an ice bath. Since the oligo contained thiol modifiers in a disulfide form, a TCEP-based chemical reduction was needed. Therefore, the pre-heated thiolated-ssDNA was mixed in a TE buffer-based solution (pH 7.5) that contained 10 mM TCEP final concentration to obtain a final ssDNA concentration of 50 μM . The solution was left for 50 min at RT and then, 10 μl was drop cast on the WE and left for 1 h 30 min at RT. After the covalent aptamer immobilization process, the electrodes were rinsed with TE buffer pH 7.5 solution and dried with N2. To block the surface and prevent unspecific molecule binding, 10 μl of 4 mM MCH were dropped-cast on the WE and left for 1 h at RT. Finally, the electrodes were rinsed with TE buffer solution to remove physically attached MCH, dried with N2, and stored at 4 °C until use.

2.5. UV-vis measurements and colorimetric analysis

The absorbance measurements were conducted using a UV–visible microplate spectrophotometer SPECTRAmax 384 plus. The spectrum was recorded in a wavelength range from 400 to 700 nm with a 1 or 10 nm resolution. Sterilized 96-well plates were used for all the measurements with a total volume solution of 100 μl was used. The blank used for all the measurements consisted of polystyrene beads in DI water in a concentration of 10^{11} particles/ml.

The colorimetric image analysis was performed using ImageJ software (National Institutes of Health, US). First, pictures were taken with an iPhone® 13 Pro Max camera using Manual app (© 2019 William Wilkinson), which provides complete independent control of shutter 1/125 and ISO 22 and saves images in raw DNG format. Then, each image was split into red, green, and blue (RGB) channels, where a fixed area in the center of the circles (testing and control/reference areas) of 37×37 pixels was chosen to create gray color profiles. Finally, the profiles were used to develop the colorimetric calibration curves for both microparticles systems.

2.6. Electrochemical measurements

For the electrochemical impedance spectroscopy (EIS) tests, the redox probe used was 10 mM [Ru (NH₃)₆]³⁺Cl₃] in 0.01 M PBS, where an initial DC-bias of -0.167 mV vs. reference electrode was applied for 30 s to reduce hexaammineruthenium (III) to hexaammineruthenium (II) on the working electrode's surface. Subsequently, a voltage amplitude of 5 mV was applied in a frequency range from 100 kHz to 10 Hz. The Nyquist impedance curves obtained were fitted in the ZFit tool of Multitrace® software using Randle's circuit depicted in Fig. 4 (c). The cyclic voltammetry (CV) characterization was performed within a potential window of -0.6 to 0 V vs. the lab-modified PCB electrode at 0.1 V s $^{-1}$ scan rate. All the electrochemical measurements were performed using a Multichannel PalmSens4 Potentiostat (5V-1 MHz). The sample volume used was 100 μ l for all the experiments. For the three detection systems, the detection limit was calculated as 3 σ of the blank/slope.

2.7. Selectivity and real samples tests

Selectivity studies were conducted by non-competitive assay. The interfering ions tested were selected among the heavy metals that might be found in industrial wastewater, such as $Pb^{2+}, As^{2+}, Fe^{2+}, Mg^{2+}, Zn^{2+}, Cd^{2+}, and Cu^{2+}.$ All assays were performed in triplicates. To evaluate the applications of the method in environmental water samples, tap water, and in-field water samples were obtained from a drain ditch in the Throckmorton Purdue Agricultural Center.

3. Results and discussion

3.1. Characterization of Ps-AuNPs and Ps-AgNPs microparticles

Ps-AuNPs and Ps-AgNPs microparticles were synthesized and assessed through transmission electron microscopy (TEM). Figure S. 4 shows the TEM images, boxplots, and values of the diameter of polystyrene beads (406 nm, SD \pm 19.69, n=20), gold nanoparticles (10.38 nm, RSD 10.38%, n = 28), and silver nanoparticles (12.39 nm, SD \pm 6.2, n = 32). The monodispersity displayed in both systems is consistent with controlled growth synthesis processes, which is ideal to ensure reproducibility, stability, and homogeneous aptamer (ssDNA) immobilization. The peak absorbance wavelength for Ps-AgNPs and Ps-AuNPs is centered at a λ_{max} of 394 and 521 nm, respectively (see Fig. 1a and b red line). These results are in accordance with other literature reports, where similar gold-decorated polystyrene particles were employed in biosensors for pathogen detection (Jin et al., 2017). Then, after immobilizing the ssDNA and blocking the surface with BSA, both peaks slightly presented a redshift to 397 nm and 528 nm for Ps-AgNPs-ssDNA and Ps-AuNPs-ssDNA, respectively. This might be attributed to an increase in particle size dispersion and local refractive index caused after replacing the citrate capping ligand with the oligonucleotides and the TE buffer (Poon et al., 2010; Wang and Gunasekaran,)

Fig. 1c and d shows the zeta-potential (ζ) changes during the silver and gold-based microparticles fabrication process. An initial relative negative charge of -47.9 mV (SD \pm 3.77 and RSD 7.87%) was observed due to the terminal sulfate groups located on the surface of the polystyrene beads (Sofińska et al., 2016). Considering that for the synthesis of AgNPs and AuNPs, citrate ions were used as the reducing agent; at the end of their synthesis process, both silver and gold-based microparticles have a negative charged coating (Agnihotri et al., 2013; Alba-Molina et al., 2017; Grys et al., 2020). Therefore, there was a slight decrease in the initial ζ to -51.6 mV (SD \pm 4.44 and RSD 8.6%) and -51.9 mV (SD \pm 5.58 and RSD 10.75%) for the Ps-AuNPs and Ps-AgNPs, respectively. Finally, after ssDNA immobilization, the relative surface charge increased to -37.5 mV (SD \pm 4.91 and RSD 13.09%) for Ps-AuNPs-ssDNA and to -30.3 mV (SD \pm 4.43 and RSD 14.62%) for Ps-AgNPs-ssDNA. This increase is expected as aptamers are less negatively charged in comparison to double-stranded DNA, and their adsorption might be through phosphate anions' electrostatic interaction with the surface of pH-treated Ps-AuNPs/Ps-AgNPs. Furthermore, ssDNA can uncoil sufficiently to expose their bases compared to dsDNA, which only exposes the negatively charged phosphate-backbone. This uncoiling favors the electrostatic interaction of ssDNA with citrate-capped silver and gold nanoparticles, which ultimately leads to strong absorption of the unmodified nanoparticles (L. Li et al., 2009). Similar results have been obtained by Mohammed et al. (2019), Tanner et al. (2017), Truong et al. (2021), Ye et al. (2018). Overall, both modified microparticles' had a ζ potential greater than ± 30 mV, suggesting high colloidal stability (Sun et al., 2016). Even though the negatively charged Ag and Au nanoparticles are electrostatically preventing the adsorption of the negatively charged DNA, in the light of prior literature reports, it is indeed expected that the surface plasmon peaks shift. The loss of negative surface charged occurred as aptamer occupied the citrate sites in both microparticles, and adsorption might be achieved by nonionic forces (Mereuta et al., 2020; Truong et al.,

2021; Zhang et al., 2012a).

Literature also suggests that ssDNA can sufficiently uncoil to expose its bases and electrostatically adsorb onto the gold nanoparticle surfaces (Cho et al., 2008). However, the net negative charge provided by the citrate ions at a pH of 7.5, which is the normal pH where the aptamers are stored, does not facilitate the electrostatic adsorption of negatively charged ssDNA. Hence, treating the nanoparticles was necessary to reduce or neutralize the citrate ions on the nanoparticles' surface. To do so, we decreased the pH of the TE buffer solution, so more hydrons were available to aid in the neutralization process (Zhang et al., 2012a, 2012b, 2012a). Figure S. 3 shows that by decreasing the pH of Ps-AuNPs solution to 4.5, 5.5, 6.5, and 7.5, there is no significant color, absorbance, or redshift changes.

Nevertheless, at a pH of 3.5, the solution turns from pink to purple, and there is a significant reduction in the absorbance accompanied by redshift. This suggests that the partial or complete neutralization of citrate ions at this pH or below disfavors the electrostatic repulsion and

stabilization of the particles, leading to agglomeration. Therefore, to favor the adsorption but avoid premature aggregation, a pH of 5.5 was used for the ssDNA immobilization process.

3.2. Colorimetric detection of Hg^{2+} in solution

As a proof of concept, colorimetric detection of Hg²⁺ was performed in solution and assessed through UV–vis spectrophotometry. A vast prior body of work has used sodium chloride (NaCl) to induce ion-mediated aggregation in metal nanoparticles coated by citrate ions (Christau et al., 2017; Pamies et al., n.d.). The role of citrate ions is to provide electrostatic repulsion and stability to metal nanoparticles; however, if the aqueous medium that contains them has sufficient ionic strength (i. e., NaCl), the salt will disrupt the surface electron charge over their surface, leading to aggregation. Here, we took advantage of that phenomenon to evaluate Ps-AuNPs and Ps-AgNPs microparticles aggregation with and without aptamer (ssDNA). To do so, Ps-AuNPs without

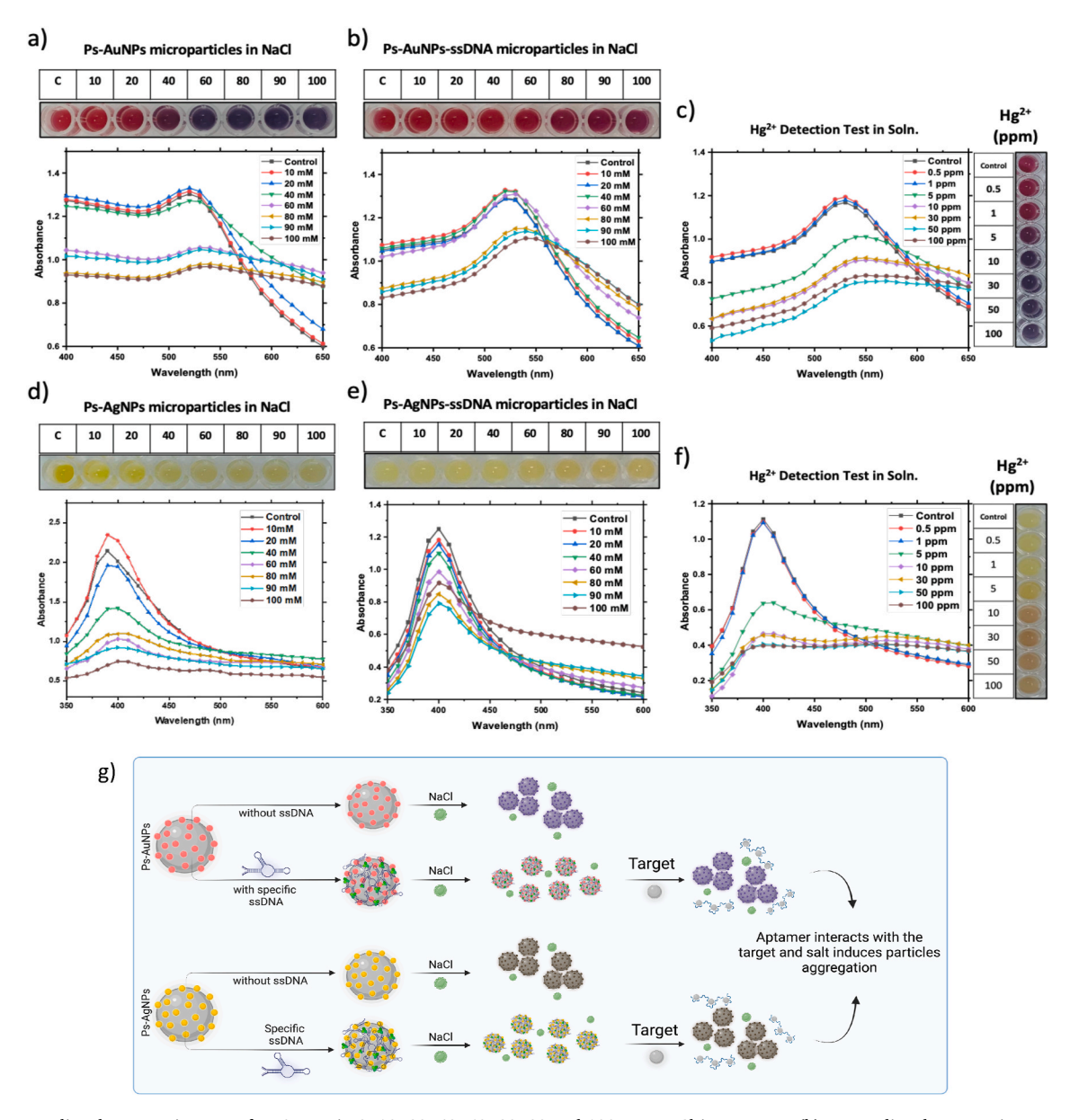


Fig. 2. (a) Ion mediated aggregation test of Ps-AuNPs in 0, 10, 20, 40, 60, 80, 90 and 100 mM NaCl in DI water, (b) Ion mediated aggregation test of Ps-AuNPs-ssDNA-BSA in 0, 10, 20, 40, 60, 80, 90 and 100 mM, (c) Hg²⁺ detection using Ps-AuNPs-ssDNA-BSA microparticles, (d) Ion mediated aggregation test of Ps-AgNPs in 0, 10, 20, 40, 60, 80, 90 and 100 mM NaCl in DI water, (b) Ion mediated aggregation test of Ps-AgNPs-ssDNA-BSA in 0, 10, 20, 40, 60, 80, 90 and 100 mM, (c) Hg²⁺ detection using Ps-AgNPs-ssDNA-BSA microparticles, UV-vis spectra (bottom) and photograph (top) of each test.

ssDNA were first exposed to different concentrations of sodium chloride (NaCl), and the UV–vis spectra was used to examine the spectral changes of the surface plasmon bands.

Aggregation in gold nanoparticles is known to result in a redshift in a UV-vis absorption spectrum and a decrease in the absorption spectra due to a reduction in the interparticle distance and the dilution effect, respectively (Alba-Molina et al., 2017; Cho et al., 2008). Fig. 2a shows a negligible change in UV-vis spectra upon adding NaCl from 10 to 40 mM, suggesting that Ps-AuNPs microparticles do not aggregate at these concentrations. At 40 mM, there was a slight redshift, but it was not significant enough, and the particles were still stable. However, at concentrations beyond 60 mM, a change in color from pink to purple can be observed because at higher salt concentrations, the electrostatic repulsion is reduced as the dissociative ions shelter the surface charge on the AuNPs, which leads to aggregation. Similarly, Fig. 2b shows the UV-vis spectra of Ps-AuNPs-ssDNA microparticles in the presence of NaCl at different concentrations. In this case, particles remained stable up to 60 mM salt concentration, which might support that the ssDNA surface modification on Ps-AuNPs has taken place as the particles showed more resistance to the NaCl ion sheltering effect (Li and Roth-

Fig. 2c shows the UV-vis spectra and color change of Ps-AuNPs-ssDNA in the presence of Hg^{2+} . Thymine-rich ssDNA was used as the aptamer of Hg^{2+} , as it can strongly bind to thymine and form T-Hg-T complexes. The detection mechanism for both microparticles is

described in Fig. 2g. It can be observed that to destabilize selectively and sensitively aggregate Ps-AuNPs/AgNPs-ssDNA in the presence of Hg^{2+} , a fixed concentration of salt (60 mM) is required to trigger particles' aggregation after the aptamer-target interaction. Literature reports suggest that for both types of functional microparticles, a double-stranded DNA (dsDNA) was formed in the presence of Hg^{2+} due to the thymine - Hg^{2+} -thymine (T- Hg^{2+} -T) interaction (Cui et al., 2015; Xing et al., n.d.). The formed dsDNA can easily desorb from the surface of the reported particles and induce aggregation due to the presence of salt. For the Ps-AuNPs-ssDNA colorimetric system, with the increase of Hg^{2+} concentrations, the color gradually turned purple (positive to target), suggesting an increase in the aggregation of Ps-AuNPs as the ssDNA- Hg^{2+} binding was taking place. Similar results were obtained with Ps-AgNPs and Ps-AgNPs-ssDNA (Fig. 2 d, e, and f), for which the color changed from yellow to brown.

3.3. Colorimetric detection using μ -PADs

To fabricate the μ -PADs, Whatman filter paper 1 was used as it has exhibited outstanding color intensity, sample flow, and porosity for detecting mercury through silver and gold-based platforms (Firdaus et al., 2019; Monisha Shrivas et al., 2021). To evaluate the overall fabrication of the colorimetric system, the Ps-AuNPs-ssDNA and Ps-AgNPs-ssDNA references were analyzed by compiling the average gray intensity of the active areas of 27 as-fabricated sensors. Fig. 3a

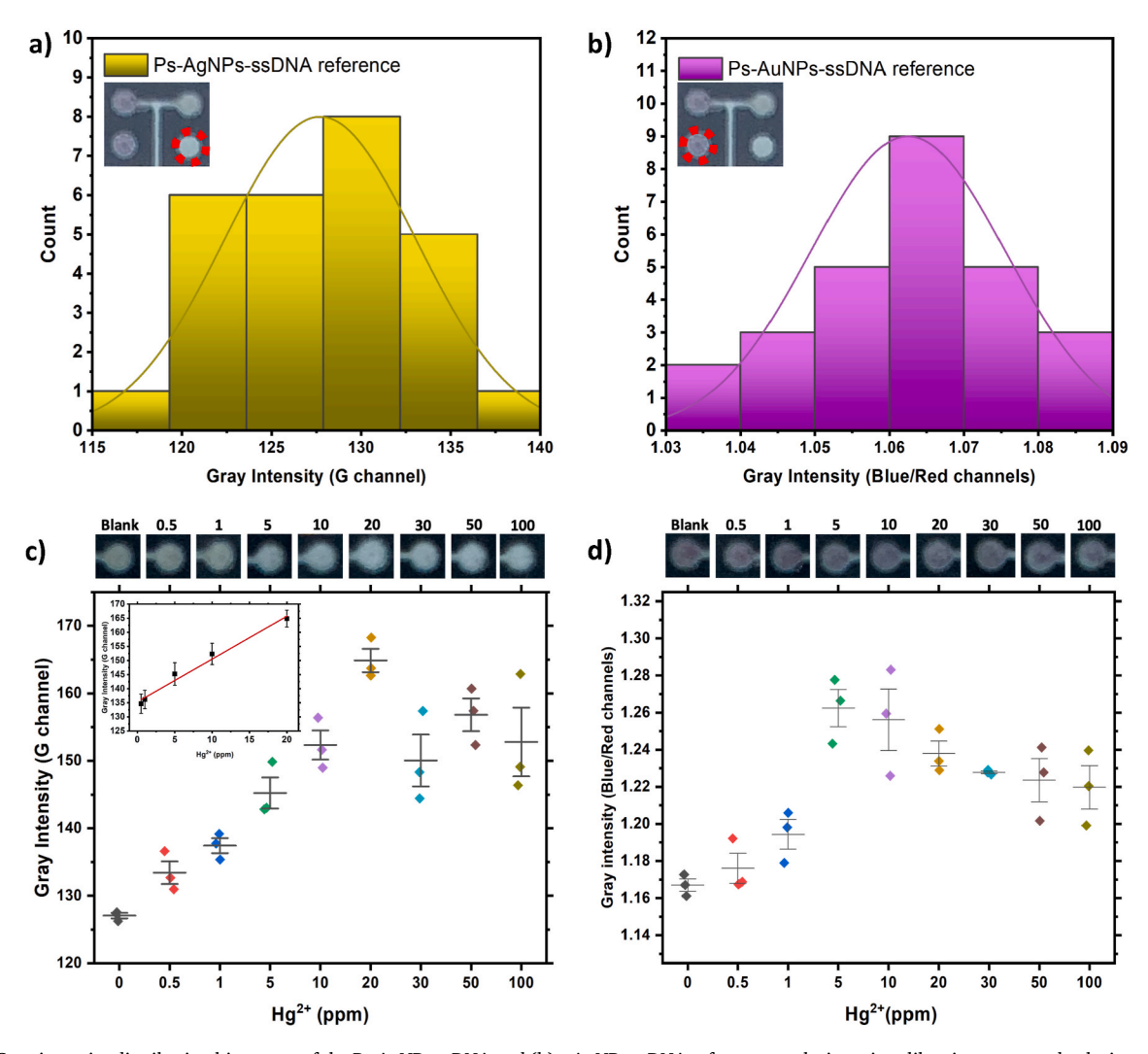


Fig. 3. (a) Gray intensity distribution histogram of the Ps-AgNPs-ssDNA and (b) s-AuNPs-ssDNA references, colorimetric calibration curve and colorimetric results on the μ -PADs obtained from the (c) Ps-AgNPs-ssDNA and (d) Ps-AuNPs-ssDNA-systems.

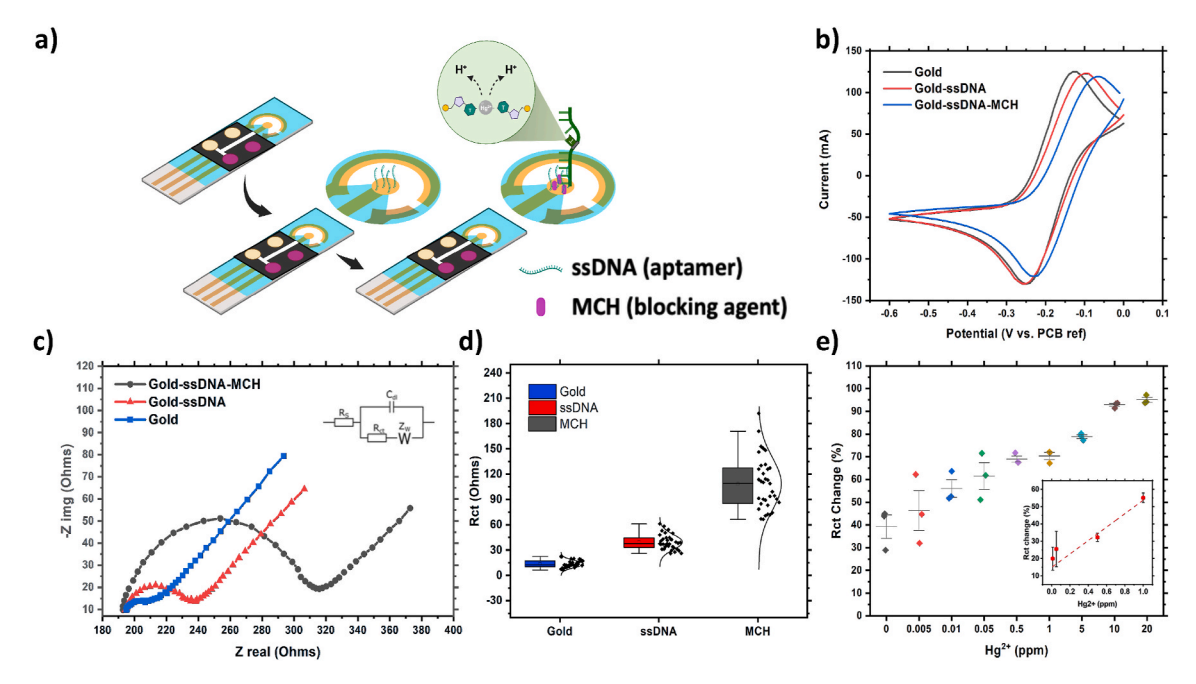


Fig. 4. a) schematic figure of surface modifications on the gold electrode, b) cyclic voltammograms and c) Nyquist plots of gold, gold-ssDNA, and gold-ssDNA-MCH, and d) charge transfer resistance box plots for each of the surface modifications (n = 25), and e) calibration curve (n = 25).

shows evidence of a controlled colorimetric signal variation with an average of 127.71 (SD \pm 5.36) and an RSD of 4.2% for the Ps-AgNPs-ssDNA system. Likewise, the Ps-AuNPs-ssDNA system (Fig. 3b) shows an average of 1.06 (SD \pm 0.013) with a controlled RSD of 1.23%. The histograms presented in Fig. 3 also demonstrate that the samples follow a mesokurtic normal-like distribution, which corroborates the reliability of the manufacturing process.

Fig. 3c shows the calibration curve for the detection of mercury using Ps-AgNPs-ssDNA particles immobilized in the μ-PAD. The fabricated paper device modified with silver-based microparticles showed the color change from yellow to colorless after the addition of Hg²⁺. The color developed on the substrate showed a linear color change in the presence of Hg^{2+} concentrations ranging from 0.5 to 20 ppm ($R^2 = 0.98$ and n =3/conc.). For this test, the mean of the gray intensity was measured using the green channel in the RGB pictures and analyzed in ImageJ. The progressive decrease from deep yellow to light yellow/white with increasing mercury concentrations suggests that not only ssDNA-target binding is taking place, but oxidation of Ag° to Ag⁺ is occurring. It has been previously reported that in solution, the presence of mercury causes aggregation of AgNPs and the yellow-brown color change (Firdaus et al., 2019). However, there is also a Redox-driven color change in paper devices from the oxidation of silver nanoparticles (Firdaus et al., 2019; Monisha Shrivas et al., 2021). The oxidation phenomenon might be attributed to the AgNPs interaction with Hg²⁺, which results from the electrostatic attraction between the negatively charged silver and the positively charged mercury, the adsorption of Hg²⁺ on the AgNPs' surface, and the amalgamation generated from also the reduction of Hg²⁺ to Hg (Vasileva et al., 2017). Due to this strong affinity and interaction of silver with mercury, the density of negative citrate ions covering the nanoparticles gradually decreases as the mercury concentration increases. The decrease of citrate ions on the particles' surface leads to their aggregation and possible sedimentation (Firdaus et al., 2019; Jarujamrus et al., 2015; Monisha Shrivas et al., 2021). Through this colorimetric method, the limit of detection (LOD) obtained was 0.5 ppm based on 3σ of the blank/slope criteria, using linear regression equations and slope of the calibration graph depicted on Fig. 3c inset plot.

To evaluate the detection performance in the testing areas, the ratio of the average gray intensities from the blue and red channels was obtained and compared. The blue/red color ratio changes upon the

exposure to Hg^{2+} in concentrations ranging from 0.5 to 100 ppm. For the Ps-AgNPs-ssDNA system, a linear correlation between Hg^{2+} concentration and gray intensity was found in the range of 0.5–20 ppm. Whereas for the Ps-AuNPs-ssDNA system, there is a significant difference in color and gray intensity between the samples used with concentrations of 0, 0.5, and 1 ppm and the samples tested with concentrations of 5 ppm and higher. The non-linear trend suggests a limitation to the quantitative detection. However, because the entire μ PAD device incorporates two colorimetric systems, it takes advantage of both. One unit allows for the qualitative identification of the analyte through colorimetric Ps-AuNPs-ssDNA changes (down to 5 ppm), and the other, Ps-AgNPs-ssDNA system, offers quantitative detection with a LOD of 0.5 ppm.

3.4. Electrochemical characterization and detection of Hg^{2+}

The stability of the fabricated AgCl PCB reference electrodes was assessed through open-circuit potential (OCP). Figure S. 6a shows the OPC obtained from sixteen PCB pseudo-reference electrodes as fabricated, which were tested against a commercial Ag/AgCl (KCl) reference electrode for 5 min using as electrolyte a calibration buffer solution of pH 7. The average relative potential value found was 46.9 \pm 6.6 mV, which is satisfactory compared to OCP values obtained in pseudoreference electrodes that have been modified through more complex processes such as electroplating (Rohaizad et al., 2019). Furthermore, OPC results show a stable electrical behavior and no significant relative potential drift during the 5 min. It is worth mentioning that upon initial contact with the electrolyte, a set-up time of \sim 3 min was required for the OCP to stabilize. Furthermore, to evaluate their performance against the PCB working electrode, EIS studies were carried out using the PCB three-electrode system, together with either a commercial Ag/AgCl reference electrode or our PCB Ag/AgCl pseudo-reference electrode. Figure S. 6 b demonstrates no significant change performance when comparing the charge transfer resistance (Rct) values of the working electrode against the commercial and the PCB electrodes and their variation over time.

CV and EIS were used to study the charge transfer resistance (Rct) of the PCB working electrode after immobilizing 50 μ M of ssDNA and 4 mM of MCH coatings. The Nyquist impedance curves obtained are shown in Fig. 4c, and they were fitted in the ZFit tool of EC-Lab software using

Randle's circuit depicted in the top right corner. In this circuit, Rs represents the electrolyte resistance, Rct represents the charge transfer resistance at the working electrode (WE) surface, Cdl is the double-layer capacitance, and Zw is the Warburg impedance element (straight line with a slope of 45°). The complete surface modification process compared the mean charge transfer resistance (Rct) values obtained from 35 electrodes. The values were 13.49 Ω (SD \pm 4.25 and RSD 31.5%) for the PCB gold electrodes after the cleaning process, 39.47 Ω (SD \pm 8.8 and RSD 22.3%) after covalently immobilizing ssDNA, and 108.5 Ω (SD \pm 31.14 and RSD 28.7%) after blocking the surface (Fig. 4d). Furthermore, one-way ANOVA statistical analysis revealed a significant difference between the different electrode groups with an $F_{2.102}$ value of 237.2, $P = 2 \times 10{\text -}16$, and R^2 of 0.82. As expected, the Rct for the PCB gold bare electrode increases after adding the ssDNA coating due to the low electrical conductivity of the oligonucleotide, and it increases further after blocking the surface with 6-mercapto-1-hexanol (MCH). For the CV characterization, the same redox probe was used, and the voltammograms for gold, gold-ssDNA, and gold-ssDNA-MCH were recorded at a potential window from -0.6 to 0 V at a scan rate of 100 mV/s (Fig. 4b). Anodic peaks in the fourth cycle were compared, the current values were 0.152 mA (SD \pm 0.001 and RSD 0.65%) for the gold electrode, 0.146 mA (SD \pm 0.005 and RSD 3.42%) for gold-ssDNA, and 0.136 mA (SD \pm 0.006 and RSD 4.41%) for gold-ssDNA-MCH. Results are correlated with EIS measurements where the highest current flow was found in the PCB gold electrode, and it decreases after the ssDNA and blocking immobilization coatings are incorporated.

Fig. 4e shows the Hg^{2+} calibration curve based on the charge transfer resistance change (ΔRct) before and after adding the target at concentrations of 0.005, 0.01, 0.5, 1, 5, 10, and 20 ppm. The detection limit was 0.01 ppm as 3σ of the blank/slope. Due to the electrochemical techniques' highest sensitivity compared to the paper-based colorimetric platforms, a linear correlation between Log of Hg^{2+} concentrations and ΔRct was found in a range from 0.001 to 1 ppm, with an R^2 of 0.935. The thiolated ssDNA used for the electrochemical detection had the same sequence as the one used to modify the Ps-AgNPs/Ps-AuNPs microparticles. These results suggest that mercury-ssDNA interaction (thymine Hg^{2+} -thymine) might induce ssDNA conformational changes from a linear to a hairpin structure that reduced the electron transfer, which led

to an increase in the final ΔRct on the surface of the electrode (Fig. 4a and Fig. S. 7).

3.5. Selectivity and stability

To test the selectivity of the aptamer (ssDNA) towards mercury, ssDNA modified Ps-AuNPs microparticles were mixed with 60 mM NaCl and tested with the other metallic cations (10 ppm) in solution. Fig. 5d shows the UV-vis spectrum and real pictures of the solutions. No visible color or absorbance/wavelength changes were observed when As²⁺, Cu²⁺, Zn²⁺, Pb²⁺, Cd²⁺, Mg²⁺, and Fe²⁺ reacted with the Ps-AuNPsssDNA solution. However, when Hg^{2+} was added, a remarkable visible color change from pink to purple was observed, along with a reduction in the absorbance intensity and a right shift of the peak in the UV-vis spectra (see Fig. 5d orange dotted line). Similar results were obtained with the Ps-AuNPs-ssDNA microparticles immobilized in the μ-PAD system, in which the average gray intensity generated for all the other analytes with a 5 ppm concentration was only ~ 0.02 in comparison to the blank, whereas for ${\rm Hg}^{2+}$ it was 0.26 (Fig. 5b). This interaction of Ps-AuNPs-ssDNA with ${\rm Hg}^{2+}$ demonstrated the high specificity of the ssDNA. Here, Hg²⁺ can bind specifically with two DNA thymine bases (T) to form a HgII-mediated base pair, thymine-HgII-thymine (T-Hg²⁺-T), and stabilize the DNA duplexes (Lee et al., 2007; Xing et al., n.d.; Xuejia Xue et al., 2008). In contrast, other metal cations such as As^{2+} , Cu^{2+} , Zn^{2+} , Pb^{2+} , Cd^{2+} , Mg^{2+} , and Fe^{2+} do not show any significant effect on the ssDNA stability (Cao et al., 2009a). For the Ps-AgNPs-ssDNA microparticles system, the average gray intensity at 5ppm generated compared to the blank was approximately 5.95 for all the other analytes and 32.67 for Hg²⁺ (Fig. 5a). Finally, for the electrochemical detection method, the average charge transfer resistance change generated using 5 ppm by other analytes was 10.76 compared to the blank and 38.96 for Hg²⁺ (Fig. 5c). These results suggest that this novel hybrid electrochemical-colorimetric approach affords increased sensitivity and selectivity, as demonstrated by the low null rate of false positives and low detection limits.

In terms of stability, a total of 18 colorimetric devices were stored and tested after 3, 7, and 30 days at 4 $^{\circ}$ C of fabrication using concentrations of 0 and 5 ppm of Hg²⁺. For the colorimetric Ps-AuNPs-ssDNA

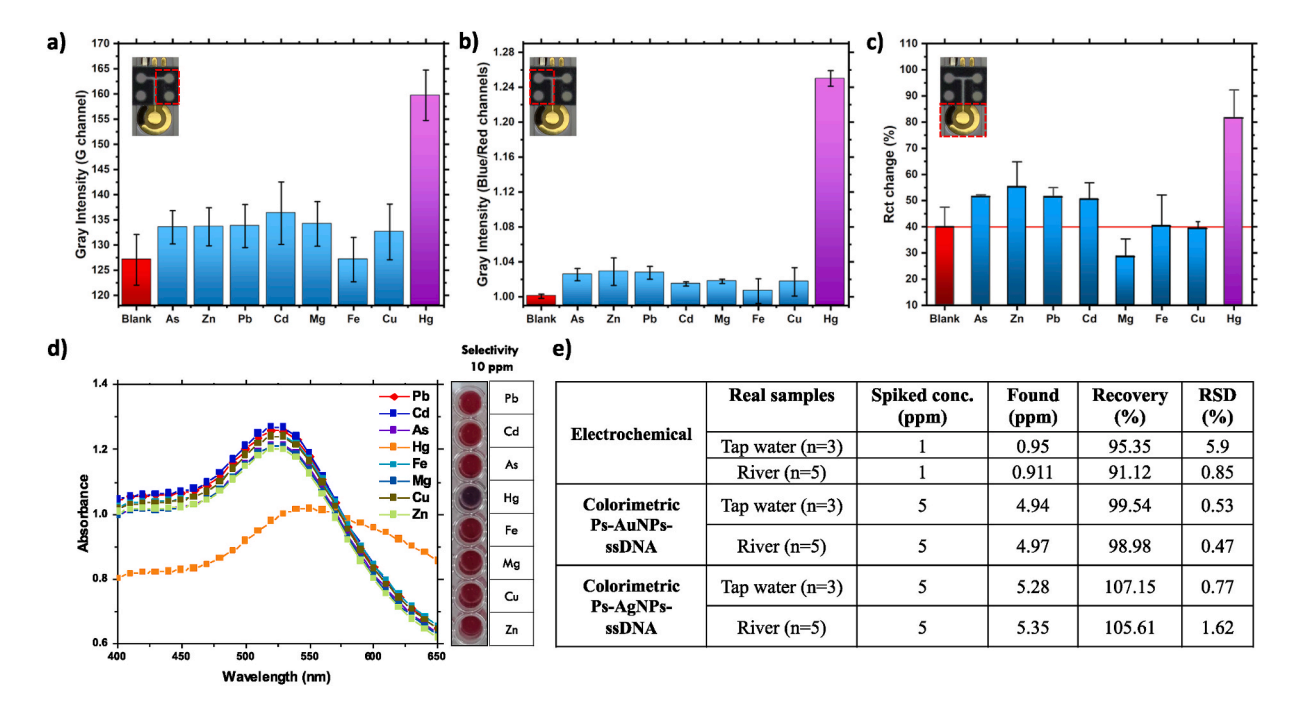


Fig. 5. Selectivity tests performed in the (a) Ps-AgNPs-ssDNA and (b) Ps-AuNPs-ssDNA modified μ-PAD, and (c) in the PCB three-electrode system using 5 ppm, (d) Ps-AuNPs-ssDNA in solution using 10 ppm concentrations of other metallic cations, and (e) results of the real sample test.

system, the average signal retention obtained with 5 ppm was 100.09, 99.67, and 98.45% (n = 3/day) after 3, 7, and 30 days, respectively. For the colorimetric Ps-AgNPs-ssDNA system the average signal retention obtained with 5 ppm was 101.98, 81.56, and 94.95% (n = 3/day) after 3, 7 and 30 days, respectively. Similar results were obtained with 0 ppm of Hg²⁺, in which an average recovery percentage of 100.1 after 3 days, 97.59 after 7 days, and 121.93 after 30 days using Ps-AuNPs-ssDNA was observed. Regarding the recovery of the Ps-AgNPs-ssDNA system at 0 ppm, the results obtained were 105.59, 83.61, and 92.77 after 3, 7, and 30 days, respectively. Finally, the stability of the electrochemical platform was evaluated after 3 and 7 days as evident damage of the PCB system was observed after 30 days due to humidity. Nevertheless, an average recovery of 100.95 (SD \pm 1.2) and 102.52 (SD \pm 11.7) was found after 3 and 7 days, respectively. These results confirmed the outstanding stability of the hybrid platform when the devices are properly stored, which is crucial to preserve the ssDNA-modified microparticles.

3.6. Real sample analysis

To test the applicability of the sensor in-field, a total of three samples of tap water and five in-field water samples obtained from a drain ditch in the Throckmorton Purdue Agricultural Center were spiked to obtain concentrations of 1 and 5 ppm. Fig. 5e shows the recovery levels achieved using electrochemical and colorimetric systems. For this purpose, the gray signal intensities and the Rct changes were compared with those achieved for standard solutions. The electrochemical approach achieved a 95.35% (RSD 5.9%) and 91.12% (RSD 0.85%) recovery for tap water and river water, respectively. Similarly, the colorimetric signal recovery using Ps-AgNPs-ssDNA microparticles was 107.15% (RSD 0.77%) for tap water samples and 105.61% (RSD 1.62%) for river water samples. Finally, recovery results of 99.54% (RSD=0.53%) for tap water and 98.98% (RSD 0.47%) for river water were shown using the Ps-AuNPs-ssDNA microparticles-based colorimetric system, which suggests positivity for mercury. Due to the qualitative discrimination provided by the gold-based microparticles, the real sample test results prove the presence of the analyte in river and tap water but do not specify its concentration.

4. Conclusion

We have reported a dual-modality, multiplex, and multi-replicate ready aptasensing platform for Hg²⁺ with an overall high sensitivity down to 0.01 ppm and selectivity against other heavy metals. The qualitative Hg2+ identification is provided by the colorimetric Ps-AuNPs-ssDNA changes and gives a negative/positive result down to 5 ppm. The electrochemical and Ps-AgNPs-ssDNA colorimetric components quantitatively measure the surface charge transfer resistance (LOD = 0.01 ppm) and color changes (LOD = 0.5 ppm) correlated to mercury concentration, respectively. We proposed a smartphone-based device for the colorimetric modality, and a miniaturized electrochemical system for a fully portable device. Therefore, the work reported herein resulted in accurate quantification of ${\rm Hg}^{2+}$ ions, even for in-field, real-world applications, such as river and tap water. The device performance in river samples is demonstrated by recovery values of up to 91.12% (RSD 0.85) and 105.61% (RSD 1.62) for the electrochemical and colorimetric components, respectively. Furthermore, the PCB incorporated into the μ-PADs helps avoid false-positive/false-negative results and thus could support future commercialization efforts. The development of this dual-mode platform opens the way to the future development of multiplexed aptamer based detection of several heavy metals, toxins, or pathogens for on-site applications.

CRediT authorship contribution statement

Ana M. Ulloa-Gomez: Conceptualization, Methodology, Validation,

Formal analysis, Investigation, Writing – original draft, Writing – review & editing, Visualization. Alec Lucas: Conceptualization, Methodology, Formal analysis, Validation, Investigation, Writing – original draft, Visualization. Abbey Koneru: Methodology, Validation, Investigation. Amit Barui: Conceptualization, Methodology. Lia Stanciu: Conceptualization, Resources, Data curation, Writing – original draft, Writing – review & editing, Validation, Supervision, Project administration, Funding acquisition.

Declaration of competing interest

The authors declare that they have no known competing financial interests or personal relationships that could have appeared to influence the work reported in this paper.

Acknowledgments

This work is supported by the U.S. Department of Agriculture, Agricultural Research Service, under Agreement ARS-CFSE funding (no. 59-8072-6-001), project [no. 8072- 42000-077-00D] and the NSF/CBET#2027554.

Appendix A. Supplementary data

Supplementary data to this article can be found online at https://doi. org/10.1016/j.bios.2022.114419.

References

- Abdollahi-Aghdam, A., Majidi, M.R., Omidi, Y., 2018. Microfluidic paper-based analytical devices (μPADs) for fast and ultrasensitive sensing of biomarkers and monitoring of diseases. Bioimpacts: BI 8, 237. https://doi.org/10.15171/
- Agnihotri, S., Mukherji, Soumyo, Mukherji, Suparna, 2013. Size-controlled silver nanoparticles synthesized over the range 5–100 nm using the same protocol and their antibacterial efficacy. RSC Adv. 4, 3974–3983. https://doi.org/10.1039/C3RA44507K.
- Alba-Molina, D., Martín-Romero, M.T., Camacho, L., Giner-Casares, J.J., 2017. Ion-mediated aggregation of gold nanoparticles for light-induced heating, 2017 Appl. Sci. 7. https://doi.org/10.3390/APP7090916, 916 7, 916.
- Arif, N., Yadav, V., Singh, Shweta, Singh, Swati, Ahmad, P., Mishra, R.K., Sharma, S., Tripathi, D.K., Dubey, N.K., Chauhan, D.K., 2016. Influence of high and low levels of plant-beneficial heavy metal ions on plant growth and development. Front. Environ. Sci. 4, 69. https://doi.org/10.3389/FENVS.2016.00069/BIBTEX.
- Mark L. Bruce and Kathleen L. Richards, Quanterra inc., 4101 shuffel dr. NW, brucem@quanterra.com, lorraine M. Miller, olin corporation, 1186 lower river road NW, Immiller@corp.olin.com, n.d. Mercury in soil screening by immunoassay [WWW document]. WTQA '98 14th Annual Waste Testing & Quality Assurance Symposium. URL https://archive.epa.gov/epawaste/hazard/web/pdf/final98a.pdf (accessed 11.10.21).
- Cao, R.G., Zhu, B., Li, J., Xu, D., 2009a. Oligonucleotides-based biosensors with high sensitivity and selectivity for mercury using electrochemical impedance spectroscopy. Electrochem. Commun. 11, 1815–1818. https://doi.org/10.1016/J. ELECOM.2009.07.029.
- Cao, R.G., Zhu, B., Li, J., Xu, D., 2009b. Oligonucleotides-based biosensors with high sensitivity and selectivity for mercury using electrochemical impedance spectroscopy. Electrochem. Commun. 11, 1815–1818. https://doi.org/10.1016/J. ELECOM.2009.07.029.
- Chaiyo, S., Apiluk, A., Siangproh, W., Chailapakul, O., 2016. High sensitivity and specificity simultaneous determination of lead, cadmium and copper using μPAD with dual electrochemical and colorimetric detection. Sensor. Actuator. B Chem. 233, 540–549. https://doi.org/10.1016/J.SNB.2016.04.109.
- Chansuvarn, W., Tuntulani, T., Imyim, A., 2015. Colorimetric detection of mercury(II) based on gold nanoparticles, fluorescent gold nanoclusters, and other gold-based nanomaterials. Trac. Trends Anal. Chem. 65, 83–96. https://doi.org/10.1016/J.TRAC.2014.10.013.
- Chen, G.-H., Chen, W.-Y., Yen, Y.-C., Wang, C.-W., Chang, H.-T., Chen, C.-F., 2014a. Detection of mercury(II) ions using colorimetric gold nanoparticles on paper-based analytical devices. Anal. Chem. 86, 6843–6849. https://doi.org/10.1021/ AC5008688.
- Chen, G.-H., Chen, W.-Y., Yen, Y.-C., Wang, C.-W., Chang, H.-T., Chen, C.-F., 2014b. Detection of mercury(II) ions using colorimetric gold nanoparticles on paper-based analytical devices. Anal. Chem. 86, 6843–6849. https://doi.org/10.1021/ AC5008688
- Cho, K., Lee, Y., Lee, C.H., Lee, K., Kim, Y., Choi, H., Ryu, P.D., Lee, S.Y., Joo, S.W., 2008. Selective aggregation mechanism of unmodified gold nanoparticles in detection of

- single nucleotide polymorphism. J. Phys. Chem. C 112, 8629–8633. https://doi.org/
- Christau, S., Moeller, T., Genzer, J., Koehler, R., von Klitzing, R., 2017. Salt-induced aggregation of negatively charged gold nanoparticles confined in a polymer brush matrix. Macromolecules 50, 7333–7343. https://doi.org/10.1021/ACS. MACROMOL.7B00866/SUPPL_FILE/MA7B00866_SI_001.PDF.
- Chwastowska, J., Skwara, W., Sterlińska, E., Pszonicki, L., 2005. Speciation of chromium in mineral waters and salinas by solid-phase extraction and graphite furnace atomic absorption spectrometry. Talanta 66, 1345–1349. https://doi.org/10.1016/J. TALANTA.2005.01.055.
- Cui, L., Wu, J., Li, M., Ju, H., 2015. Highly sensitive electrochemical detection of mercury (II) via single ion-induced three-way junction of DNA. undefined 59, 77–80. https://doi.org/10.1016/J.ELECOM.2015.07.012.
- Ejeta, S.Y., Imae, T., 2021. Selective colorimetric and electrochemical detections of Cr (III) pollutant in water on 3-mercaptopropionic acid-functionalized gold plasmon nanoparticles. Anal. Chim. Acta 1152, 338272. https://doi.org/10.1016/J. ACA.2021.338272.
- Firdaus, M.L., Fitriani, I., Wyantuti, S., Hartati, Y.W., Khaydarov, R., Mcalister, J.A., Obata, H., Gamo, T., 2017. Colorimetric detection of mercury(II) ion in aqueous solution using silver nanoparticles. Anal. Sci. 33, 831–837. https://doi.org/10.2116/ ANALSCI.33.831.
- Firdaus, M.L., Aprian, A., Meileza, N., Hitsmi, M., Elvia, R., Rahmidar, L., Khaydarov, R., 2019. Smartphone coupled with a paper-based colorimetric device for sensitive and portable mercury ion sensing. Chemosensors 7. https://doi.org/10.3390/ CHEMOSENSORS7020025, 2019, 25 7, 25.
- Friedman, A.D., Kim, D., Liu, R., n.d. Highly Stable Aptamers Selected from a 2'-Fully Modified fGmH RNA Library for Targeting Biomaterials. https://doi.org/10.1016/j. biomaterials.2014.08.046.
- Grys, D.B., de Nijs, B., Salmon, A.R., Huang, J., Wang, W., Chen, W.H., Scherman, O.A., Baumberg, J.J., 2020. Citrate coordination and bridging of gold nanoparticles: the role of gold adatoms in AuNP aging. ACS Nano 14, 8689–8696. https://doi.org/ 10.1021/ACSNANO.0C03050/SUPPL_FILE/NNOC03050_SI_001.PDF.
- Han, D., Kim, Y.-R., Oh, J.-W., Hyun Kim, T., Kumar Mahajan, R., Seung Kim, J., Kim, H., 2009. A Regenerative Electrochemical Sensor Based on Oligonucleotide for the Selective Determination of mercury(II). https://doi.org/10.1039/b908457f.
- Jaishankar, M., Tseten, T., Anbalagan, N., Mathew, B.B., Beeregowda, K.N., 2014.
 Toxicity, mechanism and health effects of some heavy metals. Interdiscipl. Toxicol.
 7, 60. https://doi.org/10.2478/INTOX-2014-0009.
- Jarujamrus, P., Amatatongchai, M., Thima, A., Khongrangdee, T., Mongkontong, C., 2015. Selective colorimetric sensors based on the monitoring of an unmodified silver nanoparticles (AgNPs) reduction for a simple and rapid determination of mercury. Spectrochim. Acta Mol. Biomol. Spectrosc. 142, 86–93. https://doi.org/10.1016/J. SAA 2015.01.084
- Jin, S.A., Heo, Y., Lin, L.K., Deering, A.J., Chiu, G.T.C., Allebach, J.P., Stanciu, L.A., 2017. Gold decorated polystyrene particles for lateral flow immunodetection of Escherichia coli O157:H7. Microchim. Acta 184, 4879–4886. https://doi.org/ 10.1007/S00604-017-2524-5/FIGURES/4.
- Kulabhusan, P.K., Hussain, B., Yüce, M., 2020. Current perspectives on aptamers as diagnostic tools and therapeutic agents. Pharmaceutics 12, 1–23. https://doi.org/ 10.3390/PHARMACEUTICS12070646.
- Lee, J.-S., Han, M.S., Mirkin, C.A., 2007. Colorimetric detection of mercuric ion (Hg2+) in aqueous media using DNA-functionalized gold nanoparticles. Angew. Chem. Int. Ed. 46, 4093–4096. https://doi.org/10.1002/ANIE.200700269.
- Li, H., Rothberg, L., 2004. Colorimetric Detection of DNA Sequences Based on Electrostatic Interactions with Unmodified Gold Nanoparticles.
- Li, L., Li, B., Qi, Y., Jin, Y., 2009. Label-free aptamer-based colorimetric detection of mercury ions in aqueous media using unmodified gold nanoparticles as colorimetric probe. Anal. Bioanal. Chem. 393, 2051–2057. https://doi.org/10.1007/S00216-009-2640-0.
- Li, T., Dong, S., Wang, E., 2009. Label-Free colorimetric detection of aqueous mercury ion (Hg2+) using Hg2+-modulated G-quadruplex-based DNAzymes. Anal. Chem. 81, 2144–2149. https://doi.org/10.1021/AC900188Y.
- Li, Tao, Li, Bingling, Wang, Erkang, Dong, Shaojun, 2009. G-quadruplex-based DNAzyme for sensitive mercury detection with the naked eye. Chem. Commun. 3551–3553. https://doi.org/10.1039/B903993G.
- Mereuta, L., Asandei, A., Dragomir, I.S., Bucataru, I.C., Park, J., Ho Seo, C., Park, Y., Luchian, T., 2020. Sequence-specific Detection of Single-Stranded DNA with a Gold Nanoparticle-Protein Nanopore Approach, vol. 10, p. 11323. https://doi.org/ 10.1038/s41598-020-68258-x.
- Miyake, Y., Togashi, H., Tashiro, M., Yamaguchi, H., Oda, S., Kudo, M., Tanaka, Y., Kondo, Y., Sawa, R., Fujimoto, T., Machinami, T., Ono, A., 2006. MercuryII-mediated formation of thymine-HgII-thymine base pairs in DNA duplexes. J. Am. Chem. Soc. 128, 2172–2173. https://doi.org/10.1021/JA056354D/SU20060126_115858.PDF.
- Mohammed, A.S., Nagarjuna, R., Khaja, M.N., Ganesan, R., Ray Dutta, J., 2019. Effects of free patchy ends in ssDNA and dsDNA on gold nanoparticles in a colorimetric genesensor for Hepatitis C virus RNA. Microchim. Acta 186, 1–11. https://doi.org/ 10.1007/S00604-019-3685-1.
- Monisha Shrivas, K., Kant, T., Patel, S., Devi, R., Dahariya, N.S., Pervez, S., Deb, M.K., Rai, M.K., Rai, J., 2021. Inkjet-printed paper-based colorimetric sensor coupled with smartphone for determination of mercury (Hg2+). J. Hazard Mater. 414, 125440 https://doi.org/10.1016/J.JHAZMAT.2021.125440.

- Moschou, D., Trantidou, T., Regoutz, A., Carta, D., Morgan, H., Prodromakis, T., 2015. Surface and electrical characterization of Ag/AgCl pseudo-reference electrodes manufactured with commercially available PCB technologies. Sensors 15, 18102–18113. https://doi.org/10.3390/S150818102, 2015.
- Oberhaus, F. v, Frense, D., Beckmann, D., n.d. Immobilization Techniques for Aptamers on Gold Electrodes for the Electrochemical Detection of Proteins: A Review. https://doi.org/10.3390/bjos10050045
- Office of water regulations and standards Washington, D. 20460, 1988. Water quality standards criteria summaries: a compilation of state/federal criteria | US epa [WWW document], 4.25.19, September. URL. https://nepis.epa.gov/Exe/ZyNET.exe/00001 NC8.txt?ZyActionD=ZyDocument&Client=EPA&Index=1986%20Thru%201990 &Docs=&Query=&Time=&EndTime=&SearchMethod=1&TocRestrict=n&Toc=&TocEntry=&QField=&QFieldYear=&QFieldMonth=&QFieldDay=&Use OField=&IntOFieldOp=0&ExtOFiel
- Pamies, R., Ginés, J., Cifre, H., Fernández, V., Mar Collado-González, E.•, Guillermo, F., Bañ, D., José, •, de La Torre, G., n.d. Aggregation behaviour of gold nanoparticles in saline aqueous media. https://doi.org/10.1007/s11051-014-2376-4.
- Papamatthaiou, S., Estrela, P., Moschou, D., 123AD. Printable graphene BioFETs for DNA quantification in Lab-on-PCB microsystems. https://doi.org/10.1038/s41598-021-8 9367-1.
- Poon, L., Zandberg, W., Hsiao, D., Erno, Z., Sen, D., Gates, B.D., Branda, N.R., 2010. Photothermal Release of Single-Stranded DNA from the Surface of Gold Nanoparticles through Controlled Denaturating and AuS Bond Breaking. https://doi. org/10.1021/nn1016346.
- Rohaizad, N., Mayorga-Martinez, C.C., Novotný, F., Webster, R.D., Pumera, M., 2019. 3D-printed Ag/AgCl pseudo-reference electrodes. Electrochem. Commun. 103, 104–108. https://doi.org/10.1016/J.ELECOM.2019.05.010.
- Sofińska, K., Adamczyk, Z., Barbasz, J., 2016. Mechanism of immunoglobulin G adsorption on polystyrene microspheres. Colloids Surf. B Biointerfaces 137, 183–190. https://doi.org/10.1016/J.COLSURFB.2015.07.037.
- Song, J., Park, S., Kim, S., Im, K., Park, N., 2017. Electrostatic interaction driven gold nanoparticle assembly on three-dimensional triangular pyramid DNA nanostructures. New J. Chem. 41, 9590–9593. https://doi.org/10.1039/ C7NJ01944K.
- Sun, D., Kang, S., Liu, C., Lu, Q., Cui, L., Hu, B., 2016. Effect of zeta potential and particle size on the stability of SiO2 nanospheres as carrier for ultrasound imaging contrast agents. Int. J. Electrochem. Sci. 11, 8520–8529. https://doi.org/10.20964/ 2016.10.30.
- Tanner, E.E.L., Sokolov, S. v., Young, N.P., Compton, R.G., 2017. DNA capping agent control of electron transfer from silver nanoparticles. Phys. Chem. Chem. Phys. 19, 9733–9738. https://doi.org/10.1039/C7CP01721A.
- Tanvir, F., Yaqub, A., Tanvir, S., An, R., Anderson, W.A., 2019a. Colorimetric detection of mercury ions in water with capped silver nanoprisms. Materials 12. https://doi. org/10.3390/MA12091533.
- Tanvir, F., Yaqub, A., Tanvir, S., An, R., Anderson, W.A., 2019b. Materials Colorimetric Detection of Mercury Ions in Water with Capped Silver Nanoprisms. https://doi.org/ 10.3390/ma12091533
- Truong, P.L., Duyen, V.T.C., Toi, V. van, 2021. Rapid detection of tebuconazole based on aptasensor and aggregation of silver nanoparticles. J. Nanomater. https://doi.org/ 10.1155/2021/5532477. 2021.
- Vasileva, P., Alexandrova, T., Karadjova, I., 2017. Application of starch-stabilized silver nanoparticles as a colorimetric sensor for mercury(II) in 0.005 mol/L nitric acid. J. Chem. https://doi.org/10.1155/2017/6897960, 2017.
- Wang, Y.-C., Gunasekaran, S., n.d. Spectroscopic and microscopic investigation of gold nanoparticle nucleation and growth mechanisms using gelatin as a stabilizer. htt ps://doi.org/10.1007/s11051-012-1200-2.
- Wen, B., Shan, X.Q., Lian, J., 2002. Separation of Cr(III) and Cr(VI) in river and reservoir water with 8-hydroxyquinoline immobilized polyacrylonitrile fiber for determination by inductively coupled plasma mass spectrometry. Talanta 56, 681–687. https://doi.org/10.1016/S0039-9140(01)00632-4.
- Xing, Y., Han, J., Wu, X., Pierce, D.T., Zhao, J.X., n.d. Aggregation-based determination of mercury(II) using DNA-modified single gold nanoparticle, T-Hg(II)-T interaction, and single-particle ICP-MS. https://doi.org/10.1007/s00604-019-4057-6.
- Xue, Xuejia, Wang, Feng, Liu*, X., 2008. One-step, room temperature, colorimetric detection of mercury (Hg2+) using DNA/nanoparticle conjugates. J. Am. Chem. Soc. 130, 3244–3245. https://doi.org/10.1021/JA076716C.
- Yan, T., Zhang, G., Chai, H., Qu, L., Zhang, X., 2021. Flexible biosensors based on colorimetry, fluorescence, and electrochemistry for point-of-care testing. Front. Bioeng. Biotechnol. 9, 883. https://doi.org/10.3389/FBIOE.2021.753692/BIBTEX.
- Ye, X., Fang, X., Li, X., Kong, J., 2018. Gold nanoparticle-mediated nucleic acid isothermal amplification with enhanced specificity. Anal. Chim. Acta 1043, 150–157. https://doi.org/10.1016/J.ACA.2018.09.016.
- Zarlaida, F., Adlim, M., 1967. Gold and silver nanoparticles and indicator dyes as active agents in colorimetric spot and strip tests for mercury(II) ions: a review. Microchim. Acta. https://doi.org/10.1007/s00604-016-1967-4.
- Zhang, X., Servos, M.R., Liu, J., 2012a. Surface science of DNA adsorption onto citrate-capped gold nanoparticles. Langmuir 28, 3896–3902. https://doi.org/10.1021/LA205036P/SUPPL_FILE/LA205036P_SI_001.PDF.
- Zhang, X., Servos, M.R., Liu, J., 2012b. Instantaneous and quantitative functionalization of gold nanoparticles with thiolated DNA using a pH-assisted and surfactant-free route. J. Am. Chem. Soc. 134, 7266–7269. https://doi.org/10.1021/JA3014055/ SUPPL FILE/JA3014055 SI 001.PDF.